https://dx.doi.org/10.1016/j.envpol.2019.06.004

Atmospheric fate of peroxyacetyl nitrate in suburban Hong Kong and its impact on local ozone pollution

Lewei Zeng,[1] Gang-Jie Fan,[2] Xiaopu Lyu,[1] Hai Guo,[*,1] Jia-lin Wang,[2] Dawen Yao[1]

[1]Air Quality Studies, Department of Civil and Environmental Engineering, The Hong Kong Polytechnic University, Hong Kong, China

[2]Department of Chemistry, National Central University, Taiwan

*Corresponding author. ceguohai@polyu.edu.hk;

Abstract

Peroxyacetyl nitrate (PAN) is an important reservoir of atmospheric nitrogen, modulating reactive nitrogen cycle and ozone (O_3) formation. To understand the origins of PAN, a field measurement was conducted at Tung Chung site (TC) in suburban Hong Kong from October to November, 2016. The average level of PAN was 0.63±0.05 ppbv, with a maximum of 7.30 ppbv. Higher PAN/O_3 ratio (0.043-0.058) was captured on episodes, i.e. when hourly maximum O_3 exceeded 80 ppbv, than on non-episodes (0.01), since O_3 production was less efficient than PAN when there was an elevation of precursors (*i.e.* volatile organic compounds (VOCs) and nitrogen oxide (NO_x)). Model simulations revealed that oxidations of acetaldehyde (65.3±2.3%), methylglyoxal (MGLY, 12.7±1.2%) and other oxygenated VOCs (OVOCs) (8.0±0.6%), and radical cycling (12.2±0.8%) were the major production pathways of peroxyacetyl (PA) radical, while local PAN formation was controlled by both VOCs and NO_2. Among all VOC species, carbonyls made the highest contribution (59%) to PAN formation, followed by aromatics (26%) and biogenic VOCs (BVOCs) (10%) through direct oxidation/decomposition. Besides, active VOCs (*i.e.* carbonyls, aromatics, BVOCs and alkenes/alkynes) could stimulate hydroxyl (OH) production, thus indirectly facilitating the PAN formation. Apart from primary emissions, carbonyls were also generated from oxidation of first-generation precursors, *i.e.*, hydrocarbons, of which xylenes contributed the most to PAN production. Furthermore, PAN formation suppressed local O_3 formation at a rate of 2.84 ppbv/ppbv, when NO_2, OH and hydroperoxy (HO_2) levels decreased and NO value enhanced. Namely, O_3 was reduced by 2.84 ppbv per ppbv PAN formation. Net O_3 production rate was weakened (~36%) due to PAN photochemistry, so as each individual production and loss pathway. The findings advanced our knowledge of atmospheric PAN and its impact on O_3 production.

Keywords: Photochemical smog; Master Chemical Mechanism (MCM); Precursors; Formation pathways; O_3 formation

Capsule: Local O_3 formation was weakened by *in-situ* PAN formation, mostly driven by carbonyls through their direct decomposition and facilitation on OH concentration in suburban Hong Kong.

1. Introduction

Peroxyacetyl nitrate (PAN) is an important air pollutant in photochemical smog. It causes human eye irritation and affects vegetation growth (Stephens, 1969; Zhang et al., 2019) when it reaches a high concentration. It also plays a significant role in atmospheric chemistry by acting as a temporary reservoir of nitrogen oxides (NO_x) (Singh and Hanst, 1981; Fischer et al., 2014; Toma et al., 2019). It can be produced in urbanized region and decomposed into NO_x and PA (CH_3CO_3) radical in remote region after long-range transport, thus redistributing NO_x and modulating ozone (O_3) production at regional and even global scale (Singh et al., 1986; Honrath et al., 1996; Bertram et al., 2013). Therefore, understanding the formation mechanism of PAN and its impact on regional O_3 pollution is of great necessity.

PAN in the atmosphere is solely derived from photochemical reactions between volatile organic compounds (VOCs) and NO_x (Lonneman et al., 1976; Han et al., 2017). However, not all the VOC species participate in the PAN formation but those which generate PA radical, and then combine with NO_2 to form PAN. PA radical can be directly generated from the oxidation of a subset of hydrocarbons (HCs) and oxygenated VOCs (OVOCs), *i.e.* acetaldehyde, acetone, methacrolein (MACR), methyl vinyl ketone (MVK), methyl ethyl ketone (MEK) and methylglyoxal (MGLY). Apart from primary emissions, these OVOCs are secondarily formed via the oxidation of HCs, *i.e.* isoprene, acetylene, propane and some aromatics, and we treated these HCs as first-generation precursors of PAN hereafter (Liu et al., 2010; Xue et al., 2014). In contrast, thermal decomposition is the predominant sink of PAN (Zhang et al., 2015a), followed by the oxidation of OH radical.

Observed PAN values in previous studies spanned from tens of pptv to tens of ppbv at various sampling sites and usually showed a peak at midday (Grosjean et al., 2001, 2002; Lee et al., 2008; Zhang et al., 2009; Moore et al., 2010; Malley et al., 2016), reflecting its feature of secondary formation. Positive correlations of PAN with HCs and OVOCs were found in chamber experiments (Tanner et al., 1988) and field measurements (Roberts et al., 2001; Toma et al., 2019), indicating that HCs and OVOCs serve as important precursors of PAN and/or share similar

formation pathways. Moreover, simulation of a steady-state model showed that 45.7% of PA radicals were attributed to oxidation of acetaldehyde and 34.8% was isoprene-derived (LaFranchi et al., 2009), while applications of kinetic models and chemical transport models revealed important contributions of aromatics and alkenes to PAN formation in urban areas of Brazil and China (Grosjean et al., 2002; Liu et al., 2010). In addition, a photochemical box model with the master chemical mechanism was used to investigate the PAN formation in urban Beijing (Xue et al., 2014), and in Pearl River Delta (PRD) region of southern China (Yuan et al., 2018). These studies specified the dominant pathways to form PA radical (hence PAN), and the key precursors of PAN during the sampling period. However, they did not conduct in-depth investigation on the formation mechanisms of PAN under different pollution scenarios.

Apart from local formation, horizontal regional transport (Lee et al., 2012) and vertical exchange with upper atmosphere (Qiu et al., 2019) are other sources of PAN. Field measurements in Beijing revealed that high concentrations of PAN were mainly related to air masses from the south, where more polluted regions were located (Gao et al., 2014; Zhang et al., 2017). Xu et al. (2015) measured PAN at a background site in PRD and identified the influence of maritime air and continental air from both southern China and eastern China. The contribution of regional transport to PAN in PRD was further confirmed by the process analysis in the Weather Research and Forecasting-Community Multiscale Air Quality (WRF-CMAQ) model (Yuan et al., 2018).

Being produced alongside O_3 through photochemical reactions between VOCs and NO_x, PAN suppresses the O_3 formation due to their competitive relationships in polluted regions, whereas decomposition of regionally-transported PAN fuels the O_3 formation by supplying precursors (*i.e.* NO_2 and radicals) in remote low-NO_x regions. Despite the growing concerns about photochemical pollution, a handful of studies have been focused on PAN in Hong Kong and the adjoining PRD region. The only previous work reported in this region was mainly focused on the relationship of PAN with its precursors. This study was the first attempt to comprehensively look into the formation mechanism of PAN and its quantitative impact on local O_3 formation in Hong Kong.

2. Methodology

2.1 Sample collection and analysis

In this study, field measurement was carried out in suburban Hong Kong (Tung Chung, TC) from 18 October to 19 November, 2016. Figure S1 shows the geographical location of the sampling site

(22.28°N, 113.94°E). The TC site was located in northwestern Hong Kong, adjacent to the Pearl River Estuary (PRE) and surrounded by newly developed residential town. The whole sampling was conducted on the rooftop of a six-floor building, approximately 20 m height. Early studies revealed that air quality at TC was affected not only by local emissions but also by regional transport, especially in autumn, when northerly/northeasterly winds dominated (Wang et al., 2005; Guo et al., 2006). Elevated secondary pollutants (*i.e.* O_3 and PAN) and their precursors (*i.e.* VOCs and NO_x) were frequently observed at this site when air masses were from inland PRD region and/or the weather conditions were favorable for photochemical formation (Wang et al., 2009; Wang et al., 2017).

During the whole sampling period, PAN was continuously measured using an automatic PAN analyzer (Meteorology Consult Inc.) containing gas chromatography-electron captured detector (GC-ECD), and was quantified every 10 minutes. In addition, hourly whole-air samples were collected using 2 L cleaned and vacuumed stainless steel canisters from 7:00 to 19:00 on 13 sampling days, with a sampling flow rate of ~35 mL/min. During the 7 intensive sampling days (Oct. 31, Nov. 4, 5, 6, 14, 15 and 17), which were predicted as O_3 episodes with hourly maximum O_3 exceeding 80 ppbv (Grade I of Ambient Air Quality Standard in China), air samples were collected every hour, different from the two-hour resolution on the 6 non-O_3 episode sampling days (Oct. 23, Nov. 1, 3, 7, 16 and 18). The prediction of O_3 episodes was based on weather forecast and numerical model simulation. In total, 130 air samples were collected and delivered to the air laboratory of the Hong Kong Polytechnic University (HKPU) for instrumental analysis of 97 VOCs. A pre-concentrator (Model 7200, Entech Instruments Inc., USA) was applied to pre-concentrate air samples before they were injected into the GC-mass selective detector/flame ionization detector/ECD (GC-MSD/FID/ECD) system. Quality control and quality assurance were conducted before/during/after chemical analysis (Zeng et al., 2018). Briefly, before sampling, all canisters were cleaned to avoid any contamination. During the chemical analysis, targeted VOCs were identified according to GC retention time and mass spectra, and were quantified according to the calibration curves. Method detection limits (MDL) of all targeted species were lower than 150 pptv. Accuracy and precision of the analyses were within 15% and 10%, respectively.

In addition, 2-h carbonyl cartridge samples were simultaneously collected every two hours from 7:00 to 19:00 using acidified 2,4-dinitrophenylhydrazine (DNPH) silica cartridges at a flow rate of ~0.5 L/min. and in total 16 OVOC samples were measured, which were analyzed using High

Performance Liquid Chromatography (HPLC) in HKPU. Typically, the detection limits of the targeted carbonyls were ~0.2 ppbv and a measurement precision was ~10%. Furthermore, trace gases (*i.e.* O_3, carbon monoxide (CO), NO-NO_2 and sulfur dioxide (SO_2)) and meteorological parameters (*i.e.* temperature, relative humidity, solar radiation, and wind speed and direction) were continuously monitored during the whole sampling period. All the online data were integrated into hourly data. Detailed description of instrumental models, analysis techniques, detection limits and data collection can be found in previous publications (Simpson et al., 2010; Zhang et al., 2012, 2015b; Wang et al., 2015; Ling et al., 2016).

2.2 Simulation of local PAN formation

Local PAN formation was simulated using a photochemical box model (PBM) incorporating a master chemical mechanism (MCM). The PBM-MCM model has been successfully developed to simulate photochemistry of secondary pollutants, *i.e.* O_3, PAN and alkyl nitrates ($RONO_2$) in many regions all over the world, including Hong Kong (representative studies have been listed in Table S1). In this study, the chemical mechanistic information was taken from a near-explicit mechanism, MCM v3.3 (*http://mcm.leeds.ac.uk/MCM*), including ~6700 species and ~17000 reactions, which considered homogeneous reactions in the boundary layer (Jenkin et al., 1997, 2003, 2015; Saunders et al., 2003). Observation data (*i.e.* NO, NO_2, SO_2, CO, 82 C_2-C_{10} VOCs and OVOCs, temperature, solar radiation and relative humidity) were input to constrain the model from 7:00 to 19:00. Physical processes, including dry deposition, aloft exchange, and atmospheric dilution caused by the variations of the planetary boundary layer height were considered in the model. In order to achieve localized and optimized simulation results for the studied area, model construction was further adjusted (see Text S1). This box model did not take the vertical/horizontal dispersion into account, which might cause discrepancy between observed and simulated data on those days with intensive regional transport.

The index of agreement (IOA) was used to evaluate the model performance (Willmott et al., 1981). Equation 1 defines the calculation of IOA, in which higher IOA ($0 < IOA < 1$) represents higher agreement between observed values (O_i) and simulated values (S_i), indicating better modeling performance:

$$IOA = 1 - \frac{\sum_{i=1}^{n}(O_i - S_i)^2}{\sum_{i=1}^{n}(|O_i - \bar{O}| + |S_i - \bar{O}|)^2} \qquad \text{(Eq. 1)}$$

where $\bar{O}$ refers to the average observed values over n samples. Figure 1 shows the observed and simulated PAN with wind speeds and directions on the 13 VOC-sampling days. Obvious underestimations were captured on episodes (i.e. Oct. 31, Nov. 4 and 15) as well as Nov. 3 when northerly/northwesterly/northeasterly, especially northwesterly winds were prevailing in daytime hours. The underestimation of PAN might be due to the contribution of regional transport (Liu et al., 2019; Guo et al., 2009; So and Wang, 2003), which was further demonstrated using observed data (see detailed description in Text S2). However, the simulated values well captured the diurnal variations of the observed PAN on non-episodes (IOA = 0.87), when local production dominated. The IOA for non-episodes was within the accepted range (0.66-0.87) in previous work (Lyu et al., 2015, 2017; Wang et al., 2017; Liu et al., 2019). To conclude, though the PBM-MCM model cannot completely reproduce the level of PAN in the atmosphere, it reasonably simulates local photochemical formation. In this study, we only focused on the local photochemistry, and formation mechanism of transported PAN in the source region was not considered.

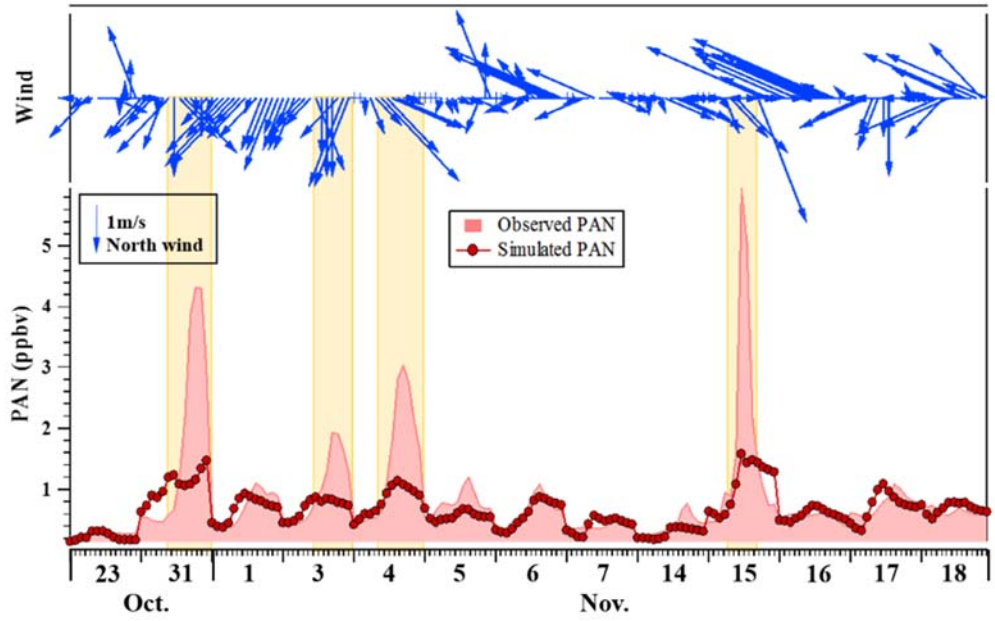

Figure 1. Observed and simulated PAN with wind speeds and wind directions (Total IOA = 0.60)

2.3 Relative Incremental Reactivity

The PAN-precursors relationship was evaluated by relative incremental reactivity (RIR), which was defined as the change of PAN formation induced by the change of mixing ratio of its precursors (NO, NO_2, and specific species/group of VOCs). If the RIR value is positive, it means that the increase of precursors enhances PAN formation, whereas negative RIR value indicated

that the increase of precursors inhibits PAN production. The RIR value was calculated from Equation 2:

$$\mathrm{RIR(X)} = \frac{[P_{PAN}(X) - P_{PAN}(X-\Delta X)]/P_{PAN}(X)}{\Delta S(X)/S(X)} \qquad \text{(Eq. 2)}$$

where X represents either a specific precursor (*e.g.* NO, NO_2 and a specific VOC) or a group of VOCs (*e.g.* aromatics and alkanes); S(X) is the measured mixing ratio of precursor X; ΔX is the change in the mixing ratio of X caused by a hypothetical change in S(X), ΔS(X); P_{PAN} is the production rate of PAN simulated by the PBM-MCM model, with a unit of pptv/h. Hourly production rate is directly extracted from the modeling results. The change in the mixing ratio of X is assumed to be 10% of the measured data.

2.4 Scenario analysis

Several scenarios were designed to evaluate the VOCs contribution to PAN formation and the impact of PAN production on local O_3 formation. Detailed model configurations for different scenarios are shown in Table S2. The Base Scenario (BS) was defined when all detected VOCs, trace gases and meteorological parameters were applied to construct the model with all reaction pathways open. Constrained Scenario 1 (CS1) was assumed to quantify the contributions of specific species/group of VOCs to PAN formation. In CS1, both formation and loss pathways of PAN remained open, consistent with the settings in the BS. However, the mixing ratios of specific species/groups of VOCs were not input into the model. Hence, their contributions to PAN formation were determined by subtracting the simulated PAN in CS1 from that in BS. The above estimated contribution included the effect of direct decomposition/oxidation of precursors (Factor 1) as well as the influence of those VOCs on OH and HO_2 concentrations (Factor 2). To separate these two contributions, Constrained Scenario 2 (CS2) was configured with similar settings to CS1, while the simulated OH and HO_2 in BS were applied to constrain OH and HO_2 in the CS2. As such, the impact of these VOCs on OH and HO_2 was eliminated, and the difference between BS and CS2 was only caused by the direct decomposition/oxidation of VOCs. Detailed description can be found in Zeng et al. (2018).

Moreover, a Constrained Scenario 3 (CS3) was designed to determine how photochemistry of PAN influenced local O_3 production. In CS3, both formation and loss pathways of PAN were closed to simulate local O_3 production without the influence of PAN. Hence, the influence of PAN formation on local O_3 photochemistry was estimated by subtracting the simulated O_3 in CS3 from that in BS.

3. Results and discussion

3.1 General characteristics

Table S3 displays the PAN mixing ratios observed in this study and in previous studies at various sampling sites. The average PAN mixing ratio at TC was 0.63±0.05 ppbv, similar to that at other suburban sites in China. Furthermore, some high values were captured during the sampling period, with a maximum value of 7.40 ppbv, implying photochemical pollution in this region, which might be attributed to not only local photochemistry, but also regional transport of polluted air masses (Xu et al., 2018), and/or evolution of planetary boundary layer in specific synoptic system (Zhang et al., 2009). Compared to previous studies, PAN level was found higher in urban and suburban areas than that at rural/background sites, due to the fact that more anthropogenic precursors were emitted in urban/suburban areas and formation of PAN dominated over the decomposition of PAN in these polluted areas, whereas its decomposition was outstanding in remote low-NO_x regions (Stockwell et al., 1995). The similar mean values of PAN (0.36-0.69 ppbv) at different rural/background sites around the world reflected its non-negligible background level.

Figure S4 shows temporal variations of PAN, O_3, NO_x, SO_2, CO, TVOCs and meteorological parameters for the whole sampling period at TC. Three days (Oct. 20 and 31, and Nov. 15) were categorized as high-pollution episodes based on the national standard of O_3 (level I hourly maximum value: 80 ppbv), on which remarkable PAN levels were observed as well, with daily maxima as 7.4, 4.3 and 6.0 ppbv, respectively. Nov. 4 was also classified as high-pollution episode, because the maximum PAN reached 2.0 ppbv. Generally, PAN correlated well (R^2=0.43) with O_3, as they share similar precursors, *i.e.* VOCs and NO_x, in photochemical formation. However, diverse PAN to O_3 ratios were found among different sampling days, particularly between episodes and non-episodes, suggesting different sources/source contributions or formation efficiencies of PAN from O_3. Figure 2 displays the diurnal variations of pollutants and meteorological parameters on episodes and non-episodes. The similar diurnal patterns of PAN and O_3 were driven by their common precursors and formation processes. Oxidation of VOCs/OVOCs by OH/NO_3 radicals led to the generation of RO_2 and HO_2 radicals, which reacted with NO resulting in O_3 formation. As an RO_2 in the O_3 formation cycle, PA radical can also react with NO_2 to produce PAN. Good correlation between PAN and O_3 indicated the dominance of local photochemistry during the sampling period. Different from O_3, which had a trough at ~8 am because of NO titration, PAN reached the trough at ~7 am due to the all-night thermal decomposition without photochemical

formation until the early morning (Zhang et al., 2015a). Peaks of both species at ~4 pm were associated with photochemical formation after sunrise and accumulation in the following hours. Average mixing ratios of PAN (1.5 ± 0.3 ppbv) and O_3 (26.9 ± 6.1 ppbv) during episodes were significantly higher ($p < 0.01$) than those during non-episodes (PAN: 0.5 ± 0.02 ppbv; O_3: 17.4 ± 1.1 ppbv), most likely related to meteorological conditions, abundance of precursors and regional transport. On episode days, higher temperature ($p < 0.01$), stronger solar radiation ($p < 0.01$), and lower humidity ($p < 0.01$) were captured in daytime hours, with larger diurnal variations, which were more favorable for photochemical formation. Moreover, precursors were much more abundant on episodes (TVOCs: 29.8 ± 3.6 ppbv; NO_2: 30.6 ± 4.0 ppbv) than those on non-episodes (TVOCs: 14.9 ± 0.9 ppbv; NO_2: 18.2 ± 0.8 ppbv) ($p < 0.01$), further fueling photochemical formation. Similarly, SO_2 (3.8 ± 0.4 ppbv) and CO (792.6 ± 29.2 ppbv) were higher on episodes than those on non-episodes (SO_2: 3.0 ± 0.1 ppbv; CO: 705.7 ± 9.2 ppbv) ($p < 0.01$), probably attributable to the increased regional transport of polluted continental air (Liu et al., 2019; Guo et al., 2009; So and Wang, 2003) or the reduced planetary boundary layer height (PBLH) on episodes or both in some cases (e.g. Oct. 20). Detailed description was presented in Text S3. In addition, though the average NO value was similar on both episodes and non-episodes owing to the different degrees of O_3 titration by NO, the morning NO peak value was higher while the afternoon values were lower on episodes, mainly due to poorer dispersion in the morning and stronger photochemical reactions (hence stronger NO titration) in daytime hours in a VOCs-limited regime.

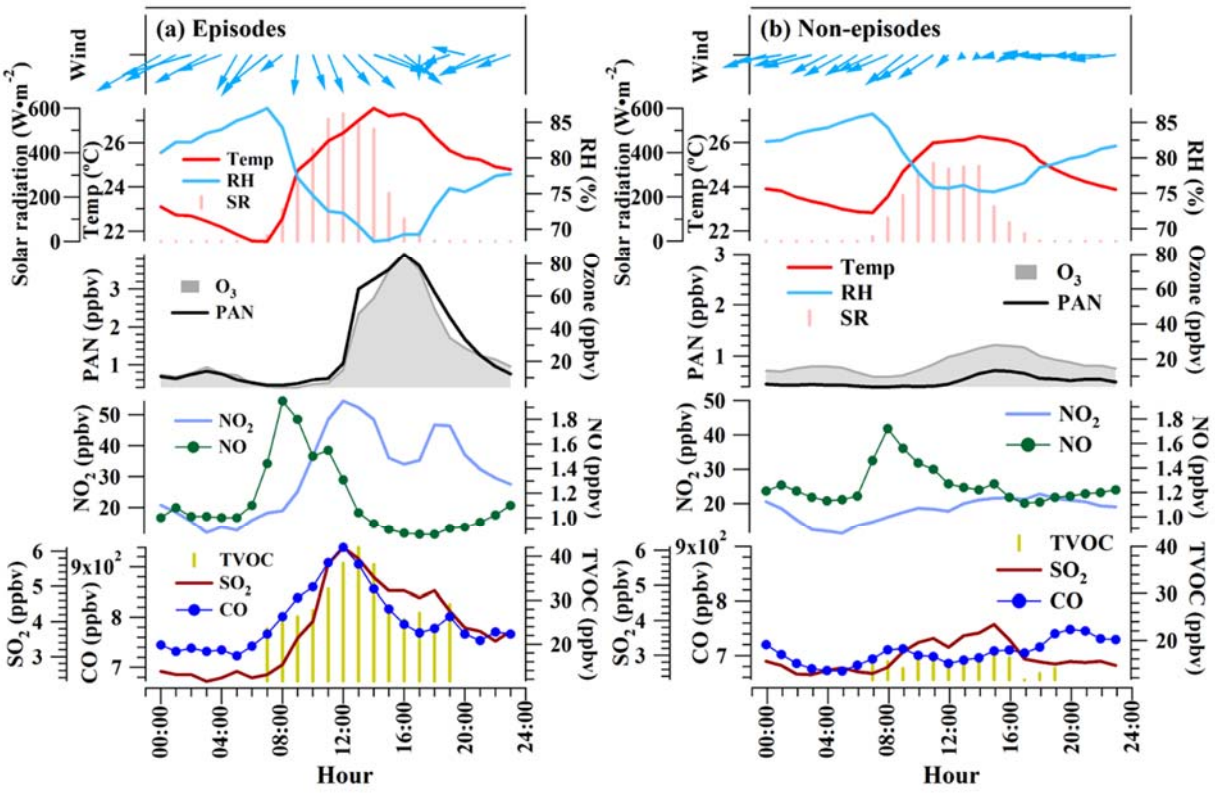

Figure 2. Diurnal trends of observed PAN, O_3, TVOCs, other trace gases and meteorological parameters on (a) episodes and (b) non-episodes

3.2 Relationship between PAN and O_3

PAN to O_3 ratio illustrates their relative photochemical production efficiencies. High PAN/O_3 was applied as an indicator for severe air pollution (Roberts et al., 1995; Stockwell et al., 1995; Zhang et al., 2014a; Liu et al., 2018). Figure 3 presents the correlations between PAN and O_3 during daytime hours (7:00-19:00) on episode and non-episode days. Clearly, high correlations were found on episode days (Oct. 20, 31, and Nov. 04, 15) with R^2 from 0.81 to 0.99, reflecting the fact that both PAN and O_3 were dominated by photochemical formation with common precursors, and/or were transported from a common source region. In contrast, correlation was poor on non-episodes (R^2 = 0.28), indicating the interference of regional transport, intrusion from upper atmosphere and background levels. The slopes of PAN to O_3 on episodes were 0.043-0.058, implying that 4.3 to 5.8 ppbv PAN were produced whenever 100 ppbv O_3 were generated via photochemical formation. In comparison, ratios on episodes found in this study were higher than those at other suburban sites, close to those obtained in urban Beijing and Ontario (Table S4), and lower than values reported in urban Lanzhou, indicating the contribution of urban air plume at TC

on episodes. In contrast, average PAN/O_3 ratio was 0.011 on non-episodes, within the range of ratios observed at other rural sites, suggesting the influence of clean air masses from coastal or marine areas. Moreover, the average NO_2 level (30.6 ± 3.9 ppbv) on episode days was much higher than that (18.2 ± 0.8 ppbv) on non-episode days ($p < 0.01$) (Figure 3). This was because NO_2 was an important precursor in PAN formation (Xue et al., 2014; Zhang et al., 2014b; Han et al., 2017). Besides, Figure S8 reveals a moderate correlation between daily averaged PAN and NO_2 in Hong Kong, with an R^2 of 0.47.

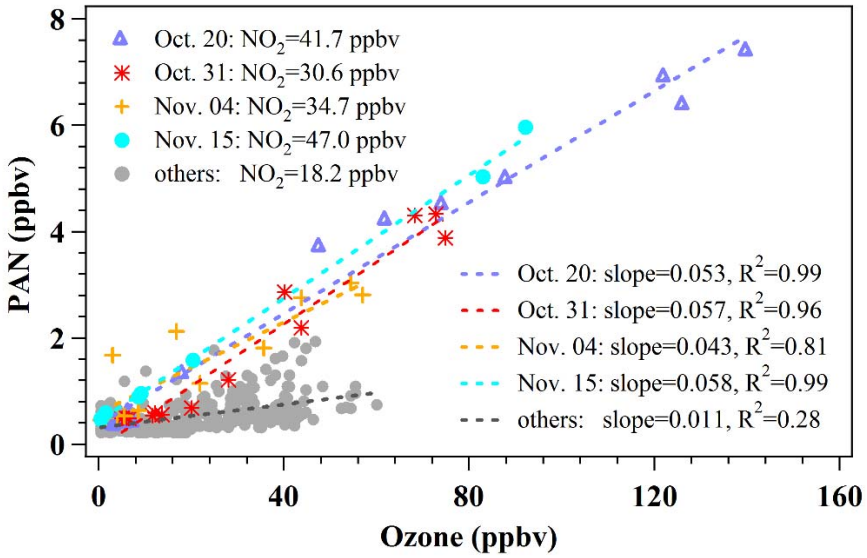

Figure 3. Relationships between daytime PAN and O_3 (7:00-19:00) on the sampling days (Gray dots for others: measurement data on non-episodes)

In general, higher PAN/O_3 was observed in more polluted air, reflecting the fact that O_3 production was less efficient than PAN (Lin et al., 1988; Roberts et al., 1995). Table 1 lists the production and destruction rates of O_3 and PAN extracted from the PBM-MCM model during episodes and non-episodes at TC. Both production and destruction processes of O_3 and PAN were enhanced on episodes, since elevated VOCs and NO_x in highly polluted air facilitated reaction cycles of O_3 and PAN. The O_3 production rate, destruction rate and net production increased only by 15%, 27% and 14% on episodes, respectively, much lower than those of PAN (145%, 149% and 127%, respectively). This was because O_3 production was dependent on NO_x conversion, and NO also titrated O_3 rapidly in the atmosphere. In contrast, increased VOCs and NO_x significantly enhanced

289 the PAN formation, since VOCs and NO_2 dominantly contributed to the sole production pathway
290 "PA + NO_2 → PAN", and the destruction rate driven by NO (~10^3 in magnitude) was negligible
291 compared to thermal decomposition (~10^6~10^7).

292

293 Table 1 Simulated production and destruction rates of O_3 and PAN during episodes and non-
294 episodes at TC

Pathway	Production and destruction rates (molecules·cm^{-3}·s^{-1})		Change
	Episodes	Non-episodes	
HO_2 + NO	1.34×10^8	1.19×10^8	13%
RO_2 + NO	2.65×10^7	2.03×10^7	31%
Gross O_3 production	1.60×10^8	1.39×10^8	15%
HO_2 + O_3	1.12×10^6	1.11×10^6	1%
O^1D + H_2O	3.79×10^6	3.12×10^6	22%
OH + O_3	8.42×10^5	7.36×10^5	14%
OH + NO_2	4.51×10^6	3.15×10^6	43%
O_3 + alkenes	2.26×10^5	1.66×10^5	36%
Gross O_3 destruction	1.05×10^7	8.28×10^6	27%
Net O_3 production	1.50×10^8	1.31×10^8	14%
PA + NO_2 **(Gross PAN production)**	1.56×10^7	6.36×10^6	145%
Thermal decomposition	1.32×10^7	5.32×10^6	149%
PAN + NO	1.63×10^3	1.04×10^3	56%
Gross PAN destruction	1.32×10^7	5.32×10^6	149%
Net PAN production	2.37×10^6	1.05×10^6	127%

295

296 ***3.3 Formation mechanism of PAN***

297 3.3.1 Formation and loss pathways of PA radical

298 Formation and loss pathways of PA radical (hence PAN) were further explored in the sampling
299 period. Note: production and destruction rates discussed here were all for locally-produced PAN
300 at TC. Figure 4 illustrates the diurnal patterns of major formation and loss pathways of PA radical
301 during episodes and non-episodes (production and destruction rates of other pathways are listed in
302 Table S5). Area shaded with solid color represented pathways derived from oxidations of

hydrocarbons or OVOCs precursors; while slash-shaded area showed the transformation between PA radical and PAN, which accounted for 62.1 ± 3.6% and 69.5 ± 2.9% of total production and destruction of PA radical in the photochemical cycling, respectively. Intensive transformation at TC was attributed to the high temperature (31.6 ± 3.3℃) during the sampling period. Except for the reactions between O_3 and C_5H_8 for PA production, and the PA destruction driven by NO_3 (Table S5), most pathways related to precursors (solid-colored) enhanced after sunrise and peaked at noontime (~12 pm). This feature was associated with the highest solar radiation at around 12 pm, when photochemical reactions became the most intensive, leading to highest simulated OH and HO_2 levels (Figure ~~S8~~S9). Instead, production rate of PA through "O_3 + C_5H_8" reached the maximum at 4 pm when the highest O_3 was observed, whereas NO_3 started to accumulate in the afternoon reaching the peak destruction rates of "PA + NO_3" at night. In addition, reaction rates of transformation between PA and PAN had high correlations with temperature (peaked at ~2pm) on both episodes (R^2 = 0.75-0.84) and non-episodes (R^2 = 0.75-0.77). Due to the combined effect of all pathways including transformation, both production and destruction of PA radical peaked at ~1 pm.

In comparison, the gross production or destruction rate of PA radical during episodes (1.86 ± 0.12 × 10^7 molecules·cm^{-3}·s^{-1}) was much higher than that on non-episodes (9.19 ± 0.05 × 10^6 molecules·cm^{-3}·s^{-1}), so was each individual pathway ($p < 0.01$). It suggested more efficient radical cycling and photochemical formation on episodes, propelled by higher temperature, stronger solar radiation and more abundant precursors.

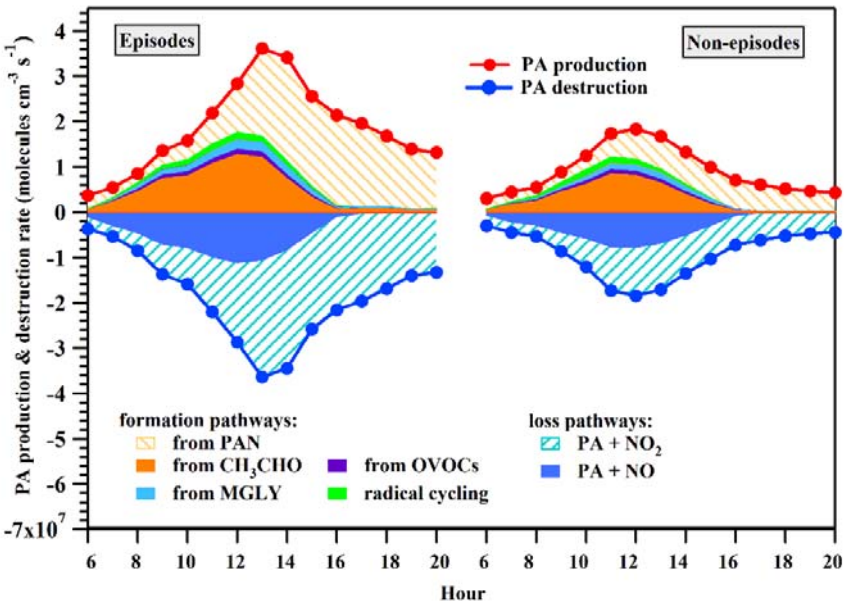

Figure 4. PA production and destruction rates of major formation and loss pathways during episode and non-episodes

For the contribution of each pathway to PA (hence PAN) production (Figure ~~S9~~S10), the transformation between PA radical and PAN was not considered so as to better investigate the role of precursors. Oxidation of acetaldehyde by OH and NO_3 was the most significant source of PA at TC, accounting for 65.3 ± 2.3%, followed by photolysis and oxidation of MGLY by OH and NO_3 with a percentage of 12.7 ± 1.2%. OH and NO_3 radicals are both important photochemical oxidants in the atmosphere, while OH outweighs NO_3 in daytime chemistry, and NO_3 plays a vital role at night (Vrekoussis et al., 2004). Propagation of other radicals to PA radical (named radical cycling hereafter), including decomposition of some larger RO/RO_2 radicals or reactions of larger acyl peroxy radicals with NO, was also an important source of PA, accounting for 12.2 ± 0.8%, while the oxidation of other OVOCs made a contribution of 8.0 ± 0.6%. Moreover, oxidation of acetone (1.2 ± 0.3%), reaction between O_3 and isoprene (0.5 ± 0.2%), and oxidation of MVK and MACR (0.1 ± 0.02%) had minor contributions to PA production. Compared to previous studies in Beijing (34.11 - 50.19%) (Xue et al., 2014) and Guangzhou (46%) (Yuan et al., 2018), acetaldehyde oxidation made larger contributions in suburban Hong Kong, likely due to a higher proportion of CH_3CHO within potential precursors (3.06 ± 0.20% in percentage and 1.51 ± 0.13 ppbv in mixing ratio). Furthermore, reaction with NO was the most predominant pathway of PA

343 destruction (99.5 ± 0.3%). No significant differences in proportions of individual pathways to PA
344 were found between episodes and non-episodes, suggesting similar pollutant profiles (composition)
345 in the atmosphere around TC.

346 Oxidation of acetaldehyde played a predominant role in PA production. Apart from primary
347 emissions, acetaldehyde can be generated through secondary formation from hydrocarbons. The
348 PBM-MCM model simulation suggested that 57.6 ± 8.2% of acetaldehyde at TC was of
349 photochemical origin (Ling et al., 2016). In addition, the other OVOCs were mainly produced
350 during the oxidation of hydrocarbons. Therefore, the identification of key first-generation
351 precursors governing PAN formation was crucial.

352 3.3.2 PAN-precursors relationship

353 Figure 5 shows the relative incremental reactivity (RIR) values of PAN precursors, including NO_x,
354 each group of VOCs, and average contribution of each VOC group to PAN. In Figure 5(a), RIRs
355 of all VOC groups were positive. Carbonyls had the highest RIR value, followed by aromatics,
356 alkenes/alkynes, BVOCs, alkanes and halocarbons. In addition, the RIR of NO was negative, while
357 NO_2 had positive RIR value. The results implied that the photochemical formation of PAN at TC
358 was mostly controlled by VOCs. It is noteworthy that NO_2 also facilitated the PAN formation,
359 which is different from O_3 formation mechanism, because NO_2 directly makes PAN while it
360 produces oxygen radical in O_3 formation. In contrast, NO inhibited PAN formation as it
361 participated in the decomposition of PAN and consumed PA radical in the atmosphere. VOCs
362 contributed to PAN formation by producing PA radical, not only in the processes of direct
363 oxidation/decomposition (Factor 1) via seven major production pathways mentioned above, but
364 also by regulating the OH concentration (Factor 2) in the atmosphere (Zeng et al., 2018). As
365 introduced in section 2.4, scenarios BS, CS1 and CS2 were performed to distinguish contributions
366 of each VOC group to PAN mixing ratio through these two factors, as shown in Figure 5(b).
367 Through direct oxidation/decomposition (Factor 1), carbonyls led to the largest increase of PAN
368 (0.34 ± 0.02 ppbv, 59 %) at TC, followed by aromatics (0.15 ± 0.02 ppbv, 26 %), BVOCs (0.06 ±
369 0.01 ppbv, 10 %), alkenes/alkynes (0.01 ± 0.002 ppbv, 2 %), alkanes (0.01 ± 0.001 ppbv, 2 %) and
370 halocarbons (0.006 ± 0.001 ppbv, 1 %), which was almost consistent with the RIR results. Besides,
371 active VOCs like carbonyls, aromatics, BVOCs and alkenes/alkynes all had large influence on
372 facilitating PAN production through building up OH concentration in suburban Hong Kong (Zeng
373 et al., 2018). In other words, their stimulation on OH abundance further enhanced the production

of PA radical. Though alkenes/alkynes were not likely to directly decompose/oxidize to form PA radical, it facilitated OH/HO_2 circulation at TC, which added up to a considerate contribution to PAN formation. Since carbonyls had both primary and secondary sources, partial carbonyls considered in the simulation came from other groups of VOCs. Hence, the contribution of carbonyls on PAN was overestimated, while there was an underestimation on those of other VOCs.

Figure ~~S10~~ S11 displays RIR values of ten key first-generation VOC species (*i.e.* hydrocarbons) governing PAN formation. Xylenes, isoprene, trimethylbenzenes, toluene, branched pentanes and $C_{2,4,5}$ alkenes/alkynes were identified as the most important PAN precursors in suburban Hong Kong. This result agreed with a previous study in suburban Beijing (Xue et al., 2014), which also proved the importance of aromatics and isoprene. Differently, this study found the significance of branched pentanes in Hong Kong.

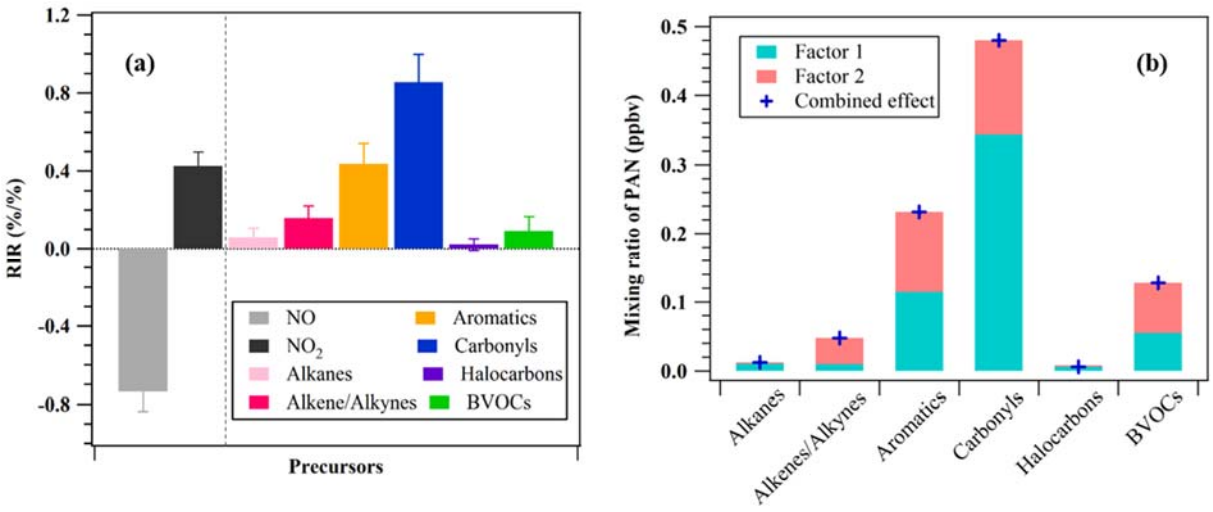

Figure 5. (a) RIR values of different VOC groups and NO_x and (b) average contributions of each VOC group to PAN at TC (Factors 1 and 2 are shown with green and red bars, respectively). Please refer to Table S6 for details of the VOC species in each group.

3.4 Impact on local O_3 formation

PAN photochemistry influences the budget of NO_x and VOCs/OVOCs that act as O_3 precursors in the troposphere, thus regulating local O_3 formation. Figure 6 shows variations of O_3, NO_2, OH and HO_2 induced by PAN formation in the daytime (7:00-19:00). The variations were derived from the differences between CS3 and BS described in section 2.4. Overall, PAN formation at TC

suppressed the local O_3 production, with an average O_3 reduction of 1.80 ± 0.25 ppbv on these days. The O_3 reduction correlated well (R^2=0.67) with the increment of PAN at a slope of 2.84 ppbv/ppbv (Figure ~~S11~~S12). In other words, O_3 was reduced by 2.84 ppbv with one ppbv PAN formation at TC. By looking into the variations of NO_x and atmospheric oxidative capacity (Figure 6), it was found that decrease in NO_2 (0.15 ± 0.04 ppbv), OH (5.00 ± 1.16×10^5 molecules·cm^{-3}) and HO_2 (2.21 ± 0.56×10^7 molecules·cm^{-3}) was driven by PAN production. Meanwhile, average NO level was enhanced by 0.16 ± 0.04 ppbv. Moreover, O_3 variation had highly positive correlations with the changes of OH (R^2 = 0.75) and HO_2 (R^2 = 0.78) radicals, and negative correlation with the NO pattern (R^2 = 0.60), suggesting the VOC-limited regime in suburban Hong Kong. It is known that PAN and O_3 formation competes for NO_2 in the photochemistry. In this study, NO_2 participated in the reaction "$NO_2 \xrightarrow{hv} NO + O$" to form O_3 and the reaction "$NO_2 + PA \rightarrow PAN$" to generate PAN, with branching ratios of 0.995 and 0.005, respectively. Solar radiation, temperature and PA concentration were the important influence factors branching these two pathways. Figure 7 displays production rates of O_3 formation/loss pathways with/without PAN photochemistry. Generally, O_3 was formed alongside the NO-NO_2 conversion in the OH-RO_2-RO-HO_2 cycle. PAN formation consumed NO_x and radicals, thus suppressing the whole cycle. This weakened both O_3 formation and loss pathways by ~33 % and ~25 % respectively, leading to reduction of O_3 production. Therefore, net O_3 production rate decreased by ~36 %. In addition, O_3 formation rates of two dominant pathways, *i.e.* "RO_2+NO" and "HO_2+NO", decreased by ~43 % and ~28 %, respectively. The dramatic weakening of "RO_2+NO" was attributable to the reduction of RO_2 (~40 %) caused by PAN photochemistry.

As the most abundant species among total peroxyacetyl nitrates (TPANs), PAN on average accounted for 40.8±2.3% of TPANs during the sampling period in suburban Hong Kong, which further implied a non-negligible contribution of TPANs to O_3 formation.

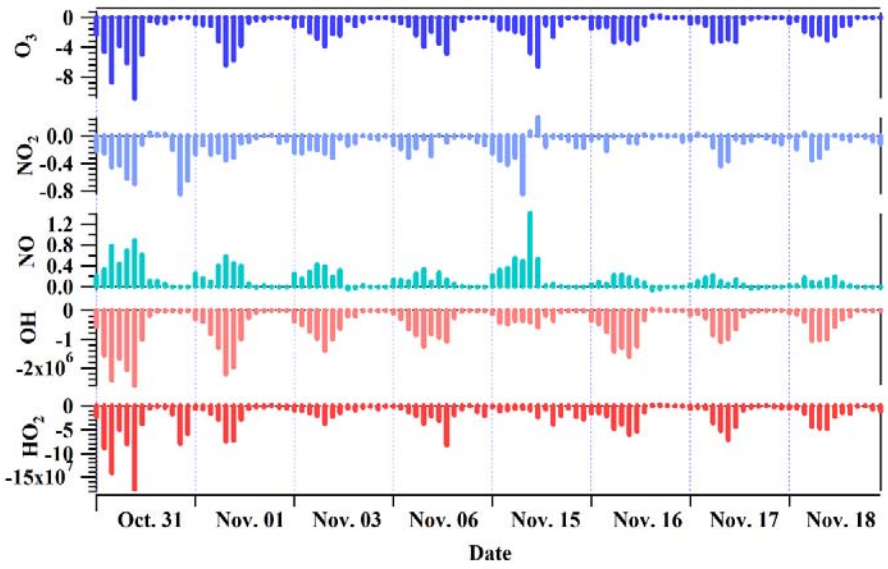

Figure 6. Variations of O_3, NO_2, NO, OH and HO_2 induced by PAN formation during 7:00-19:00 (Unit: ppbv for O_3, NO and NO_2; molecules/cm^3 for OH and HO_2)

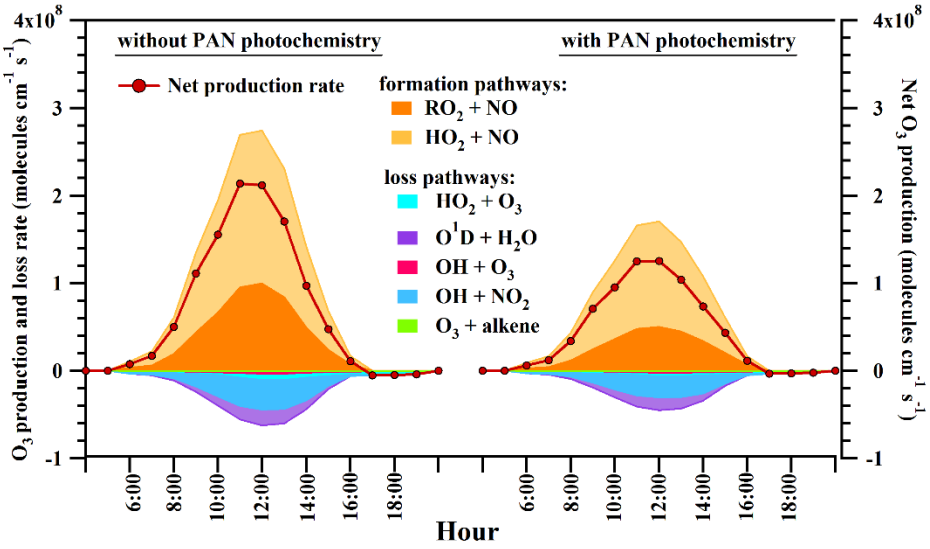

Figure 7. Formation/loss pathways of O_3 production at TC with/without PAN photochemistry

4. Conclusions

A field measurement was performed at TC site in suburban Hong Kong in autumn 2016, in order to understand the origin and atmospheric fate of PAN in this region and its influence on local O_3 formation. The average and maximum values of observed PAN were 0.63 ± 0.05 ppbv and 7.30 ppbv, respectively. Several high pollution episodes were captured with more abundant precursors

and favorable meteorological conditions, leading to more intensive *in-situ* secondary formation. Higher PAN/O_3 ratio on episodes than on non-episodes implied that O_3 production was less efficient than PAN when there was an elevation of precursors, *i.e.* VOCs and NO_x.

In-situ PAN photochemistry was investigated using the PBM-MCM model, which underestimated PAN levels during episodes due to the lack of consideration of regional transport in the model. Simulations found that except for the transformation between PA and PAN, oxidations of acetaldehyde, MGLY and other OVOCs as well as radical cycling were key pathways to form PA radical and hence PAN. Analysis of relative incremental reactivity indicated that PAN production was limited by both VOCs and NO_2 in suburban Hong Kong. Among various VOC groups, carbonyls had the highest RIR value and made the largest contribution to PAN level (0.34 ± 0.02 ppbv, 59%), followed by aromatics (0.15 ± 0.02 ppbv, 26%) and BVOCs (0.06 ± 0.01 ppbv, 10%) through direct oxidation/decomposition to form PA radical. Furthermore, active VOCs (*i.e.* carbonyls, aromatics, BVOCs, alkenes/alkynes) further facilitated PAN production through building up OH abundance in the atmosphere. In addition to primary emissions, carbonyls came from oxidations of first-generation precursors, *i.e.* hydrocarbons, mainly including aromatics, isoprene, branched pentanes and $C_{2,4,5}$ alkenes/alkynes.

Analysis on the impact of PAN on local O_3 formation revealed that the formation of PAN suppressed the HO_x and NO_2 production and increased NO level during the sampling period, leading to an O_3 reduction at a rate of 2.84 ppbv per ppbv PAN formation. Moreover, each individual production/loss pathway of O_3 was inhibited, and the net production rate decreased by ~36 % during the sampling period in suburban Hong Kong.

Acknowledgements

This study was supported by the Research Grants Council of the Hong Kong Special Administrative Region via Grants PolyU5154/13E, PolyU152052/14E, PolyU152052/16E, CRF/C5004-15E, and CRF/C5022-14G and by the Research Institute for Sustainable Urban Development of Hong Kong Polytechnic University (1-BBW4 & 1-BBW9). This study was partially supported by Hong Kong PolyU internal grants (G-YBUQ, 1-ZVJT, and 4-BCF6) and the National Key R&D Program of China (2017YFC0212001).

References

Bertram, T. H.; Perring, A. E.; Wooldridge, P. J.; Dibb, J.; Avery, M. A.;Cohen, R. C. On the export of reactive nitrogen from Asia: NOx partitioning and effects on ozone. *Atmos. Chem. Phys*. **2013**, *13*(9), 4617-4630.

Fischer, E. V.; Jacob, D. J.; Yantosca, R. M.; Sulprizio, M. P.; Millet, D. B.; Mao, J.; Paulot, F.; Singh, H. B.; Roiger, A.; Ries, L.; Talbot, R. W.; Dzepina, K.; Deolal Pandey S. Atmospheric peroxyacetyl nitrate (PAN): a global budget and source attribution. *Atmos. Chem. Phys*. **2014**, *14*(5), 2679-2698.

Gao, T. Y.; Han, L.; Wang, B.; Yang, G.; Xu, Z. Q.; Zeng, L. M.; Zhang, J. B. Peroxyacetyl nitrate observed in Beijing in August from 2005 to 2009. *J. Environ. Sci*. **2014**, 26(10), 2007-2017.

Grosjean, E.; Grosjean, D.; Woodhouse, L. F. Peroxyacetyl nitrate and peroxypropionyl nitrate during SCOS 97-NARSTO. *Environ. Sci. Technol*. **2001**, 35(20), 4007-4014.

Grosjean, E.; Grosjean, D.; Woodhouse, L. F.; Yang, Y. J. Peroxyacetyl nitrate and peroxypropionyl nitrate in Porto Alegre, Brazil. *Atmos. Environ*. **2002**, 36(14), 2405-2419.

Guo, H.; Jiang, F.; Cheng, H. R.; Simpson, I. J.; Wang, X. M.; Ding, A. J.;Wang, T. J.;Saunders, S. M.; Wang, T.; Lam, S. H. M.; Blake, D. R.; Zhang, Y. L.; Xie, M. Concurrent observations of air pollutants at two sites in the Pearl River Delta and the implication of regional transport. *Atmospheric Chemistry and Physics*. **2009**, 9(19), 7343-7360.

Guo, H.; Wang, T.; Blake, D. R.; Simpson, I. J.; Kwok, Y. H.; Li, Y. S. Regional and local contributions to ambient non-methane volatile organic compounds at a polluted rural/coastal site in Pearl River Delta, China. *Atmos. Environ*. **2006**, 40(13), 2345-2359.

Han, J.; Lee, M.; Shang, X.; Lee, G.; Emmons, L. K. Decoupling peroxyacetyl nitrate from ozone in Chinese outflows observed at Gosan Climate Observatory. *Atmos. Chem. Phys*. **2017**, 17(17), 10619-10631.

Honrath, R. E.; Hamlin, A. J.; Merrill, J. T. Transport of ozone precursors from the Arctic troposphere to the North Atlantic region. *J. Geophys. Res： Atmos*. **1996**, 101(22), 29335-29351.

Jenkin, M. E.; Young, J. C.; Rickard, A. R. The MCM v3.3.1 degradation scheme for isoprene. *Atmos. Chem. Phys*. **2015**, 15(20), 11433.

Jenkin, M. E.; Saunders, S. M.; Wagner, V.; Pilling, M. J. Protocol for the development of the Master Chemical Mechanism, MCM v3 (Part B): tropospheric degradation of aromatic volatile organic compounds. *Atmos. Chem. Phys*. **2003**, 3(1), 181-193.

Jenkin, M. E.; Saunders, S. M.; Pilling, M. J. The tropospheric degradation of volatile organic compounds: a protocol for mechanism development. *Atmos. Environ*. **1997**, 31(1), 81-104.

LaFranchi, B. W.; Wolfe, G. M.; Thornton, J. A.; Harrold, S. A.; Browne, E. C.; Min, K. E.; Wooldridge, P. J.; Gilman, J. B.; Kuster, W. C.; Goldan, P. D.; de Gouw, J. A.; McKay, M.; Goldstein, A. H.; Ren, X.; Mao, J.; Cohen, R. C. Closing the peroxy acetyl nitrate budget: observations of acyl peroxy nitrates (PAN, PPN, and MPAN) during BEARPEX 2007. *Atmos. Chem. Phys*. **2009**, 9(19), 7623-7641.

Lee, G.; Choi, H. S.; Lee, T.; Choi, J.; Park, J. S.; Ahn, J. Y. Variations of regional background peroxyacetyl nitrate in marine boundary layer over Baengyeong Island, South Korea. *Atmos. Environ*. **2012**, 61, 533-541.

Lee, G.; Jang, Y.; Lee, H.; Han, J. S.; Kim, K. R.; Lee, M. Characteristic behavior of peroxyacetyl nitrate (PAN) in Seoul megacity, Korea. *Chemosphere*. **2008**, 73 (4), 619-628.

Lin, X.; Trainer, M.; Liu, S. C. On the nonlinearity of the tropospheric ozone production. *J. Geophys. Res: Atmos*. **1988**, 93(D12), 15879-15888.

Ling, Z. H.; Guo, H.; Chen, G. X.; Lam, S. H. M.; Fan, S. J. Formaldehyde and acetaldehyde at different elevations in mountainous areas in Hong Kong. *Aerosol. Air. Qual. Res*. **2016**, 16(8), 1868-1878.

Liu, L.; Wang, X. F.; Chen, J. M.; Xue, L. K.; Wang, W. X.; Wen, L.; Li, D. D.; Chen, T. S. Understanding unusually high levels of peroxyacetyl nitrate (PAN) in winter in Urban Jinan, China. *J. Environ. Sci*. **2018**, 71, 249-260.

Liu, X.; Lyu, X.; Wang, Y.; Jiang, F.; Guo, H. Intercomparison of O_3 formation and radical chemistry in the past decade at a suburban site in Hong Kong. *Atmos. Chem. Phys*. **2019**, 19(7), 5127-5145.

Liu, Z.; Wang, Y. H.; Gu, D. A.; Zhao, C.; Huey, L. G.; Stickel, R.;Liao, J.; Shao, M.; Zhu, T.; Zeng, L. M.; Liu, S. C.; Chang, C. C.; Amoroso, A.; Costabile F. Evidence of reactive aromatics as a major source of peroxy acetyl nitrate over China. *Environ. Sci. Technol*. **2010**, 44(18), 7017-7022.

Lonneman, W. A.; Bufalini, J. J.; Seila, R. L. PAN and oxidant measurement in ambient atmospheres. *Environ. Sci. Technol*. **1976**, 10(4), 374-380.

Lyu, X. P.; Guo, H.; Wang, N.; Simpson, I. J.; Cheng, H. R.; Zeng, L. W.;Saunders, S. M.; Lam, S.; Meinardi, S.; Blake, D. R. Modeling C_1–C_4 alkyl nitrate photochemistry and their impacts on O_3 production in urban and suburban environments of Hong Kong. *J. Geophys. Res: Atmos*. **2017**, 122(19), 10539-10556.

Lyu, X. P.; Ling, Z. H.; Guo, H.; Saunders, S. M.; Lam, S. H. M.; Wang, N.; Wang, Y.; Liu, N.; Wang, T. Re-examination of C_1–C_5 alkyl nitrates in Hong Kong using an observation-based model. *Atmos. Environ*. **2015**, 120, 28-37.

Malley, C. S.; Cape, J. N.; Jones, M. R.; Leeson, S. R.; Coyle, M.; Braban, C. F.; Twigg, M. M. Regional and hemispheric influences on measured spring peroxyacetyl nitrate (PAN) mixing ratios at the Auchencorth UK EMEP supersite. *Atmos. ResAtmos. Res*. **2016**, 174, 135-141.

Moore, D. P.; Remedios, J. J. Seasonality of Peroxyacetyl nitrate (PAN) in the upper troposphere and lower stratosphere using the MIPAS-E instrument. *Atmos. Chem. Phys*. **2010**, 10(13), 6117-6128.

Qiu, Y.; Ma, Z.; Li, K. A modeling study of the peroxyacetyl nitrate (PAN) during a wintertime haze event in Beijing, China. *Sci. Total. Environ*. **2019**, 650, 1944-1953.

Roberts, J. M.; Stroud, C. A.; Jobson, B. T.; Trainer, M.; Hereid, D.; Williams, E.; Harder, H. Application of a sequential reaction model to PANs and aldehyde measurements in two urban areas. *Geophys. Res. Lett*. **2001**, 28(24), 4583-4586.

Roberts, J. M.; Tanner, R. L.; Newman, L.; Bowersox, V. C.; Bottenheim, J. W.; Anlauf, K. G.;Brice, K. A.; Parrish, D. D.; Fehsenfeld, F. C.; Buhr, M. P.; Meagher, J. F.; Bailey, E. M. Relationships between PAN and ozone at sites in eastern North America. *J. Geophys. Res: Atmospheres*. **1995**, 100(D11), 22821-22830.

Saunders, S. M.; Jenkin, M. E.; Derwent, R. G.; Pilling, M. J. Protocol for the development of the Master Chemical Mechanism, MCM v3 (Part A): tropospheric degradation of non-aromatic volatile organic compounds. *Atmos. Chem. Phys*. **2003**, 3(1), 161-180.

Simpson, I. J.; Blake, N. J.; Barletta, B.; Diskin, G. S.;Fuelberg, H. E.; Gorham, K.; Huey, L. G.; Meinardi, S.; Rowland, F. S.; Vay, S. A.; Weinheimer, A. J.; Yang, M.; Blake, D. R. Characterization of trace gases measured over Alberta oil sands mining operations: 76 speciated C_2–C_{10} volatile organic compounds (VOCs), CO_2, CH_4, CO, NO, NO_2, NO y, O_3 and SO_2. *Atmos. Chem. Phys*. **2010**, 10(23), 11931-11954.

Singh, H. B.; Salas, L. J.; Viezee, W. Global distribution of peroxyacetyl nitrate. *Nature*. **1986**, 321(6070), 588.

Singh, H. B.; Hanst, P. L. Peroxyacetyl nitrate (PAN) in the unpolluted atmosphere: An important reservoir for nitrogen oxides. *Geophys. Res. Lett*. **1981**, 8(8), 941-944.

So, K. L.; Wang, T. On the local and regional influence on ground-level ozone concentrations in Hong Kong. *Environ. Pollut*. **2003**, 123(2), 307-317.

Stephens, E. R. The formation, reaction, and properties of peroxyacyl nitrates (PANs) in photochemical air pollution. *Adv. Environ. Sci. Technoly*. **1969**, 1, 119-146.

Stockwell, W. R.; Milford, J. B.; Gao, D. F.; Yang, Y. J. The effect of acetyl peroxy-peroxy radical reactions on peroxyacetyl nitrate and ozone concentrations. *Atmos. Environ*. **1995**, 29(14), 1591-1599.

Tanner, R. L.; Miguel, A. H.; De Andrade, J. B.; Gaffney, J. S.; Streit, G. E. Atmospheric chemistry of aldehydes: enhanced peroxyacetyl nitrate formation from ethanol-fueled vehicular emissions. *Environ. Sci. Technol*. **1988**, 22(9), 1026-1034.

Toma, S.; Bertman, S.; Groff, C.; Xiong, F.; Shepson, P. B.; Romer, P.;Duffey, K.; Wooldridge, P.; Cohen,R.; Baumann, K.; Edgerton, E.; Koss, A. R.; Gouw, J.; Goldstein, A.; Hu, W.; Jimenez, J. L. Importance of biogenic volatile organic compounds to acyl peroxy nitrates (APN) production in the southeastern US during SOAS 2013. *Atmos. Chem. Phys*. **2019**, *19*(3), 1867-1880.

Vrekoussis, M.; Kanakidou, M.; Mihalopoulos, N.; Crutzen, P. J.; Lelieveld, J.; Perner, D.; Berresheim, H.; Baboukas, E. Role of the NO3 radicals in oxidation processes in the eastern Mediterranean troposphere during the MINOS campaign. *Atmos. Chem. Phys*. **2004**, 4(1), 169-182.

Wang, T.; Wei, X. L.; Ding, A. J.; Poon, S. C.; Lam, K. S.; Li, Y. S.; Chan, L. Y.; Anson, M. Increasing surface ozone concentrations in the background atmosphere of Southern China, 1994-2007. *Atmos. Chem. Phys*. **2009**, 9 (16), 6217-6227.

Wang, T.; Guo, H.; Blake, D. R.; Kwok, Y. H.; Simpson, I. J.; Li, Y. S. Measurements of trace gases in the inflow of South China Sea background air and outflow of regional pollution at Tai O, Southern China. *J. Atmos. Chem*. **2005**, 52(3), 295.

Wang, R.; Wu, T.; Dai, W. H.; Liu, H.; Zhao, J.; Wang, X.; Huang, F. Y.; Wang, Z.; Shi, C. F. Effects of straw return on C_2–C_5 non-methane hydrocarbon (NMHC) emissions from agricultural soils. *Atmos. Environ*. **2015**, 100, 210-217.

Wang, Y.; Wang, H.; Guo, H.; Lyu, X. P.; Cheng, H. R.; Ling, Z. H.; Louie P. K. K.;Simpson, I. J.; Meinardi, S.; Blake, D. R. Long-term O_3–precursor relationships in Hong Kong: field observation and model simulation. *Atmos. Chem. Phys*. **2017**, 17, 10919-10935.

Willmott, C. J. On the validation of models. *Phys. Geogr*. **1981**, 2 (2), 184-194.

Xu, X. B.; Zhang, H. L.; Lin, W. L.; Wang, Y.; Xu, W.; Jia, S. H. First simultaneous measurements of peroxyacetyl nitrate (PAN) and ozone at Nam Co in the central Tibetan Plateau: impacts from the PBL evolution and transport processes. *Atmos. Chem. Phys*. **2018**, 18(7), 5199-5217.

Xu, Z.; Xue, L. K.; Wang, T.; Xia, T.; Gao, Y.; Louie, P. K.; Luk, C. W. Measurements of peroxyacetyl nitrate at a background site in the Pearl River delta region: production efficiency and regional transport. *Aerosol. Air. Qual. Res*. **2015**, 15(1), 833-841.

Xue, L. K.; Wang, T.; Wang, X. F.; Blake, D. R.; Gao, J.; Nie, W.; Gao, R.; Gao, X. M.; Xu, Z.; Ding, A. J.; Huang, Y.; Lee, S. C.; Chen, Y. Z.; Wang, S. L.; Chai, F. H.; Zhang, Q. Z.; Wang, W. X. On the use of an explicit chemical mechanism to dissect peroxy acetyl nitrate formation. *Environ. Pollut*. **2014**, 195, 39-47.

Yuan, J.; Ling, Z. H.; Wang, Z.; Lu, X.; Fan, S. J.; He, Z. R.;Guo, H.; Wang, X. M.; Wang, N. PAN–Precursor Relationship and Process Analysis of PAN Variations in the Pearl River Delta Region. *Atmosphere*. **2018**, 9(10), 372.

Zhang, B. Y.; Zhao, X. M.; Zhang, J. B. Characteristics of peroxyacetyl nitrate pollution during a 2015 winter haze episode in Beijing. *Environ. Pollut*. **2019**, *244*, 379-387.

Zhang, B. Y.; Zhao, B.; Zuo, P.; Huang, Z.; Zhang, J. B. Ambient peroxyacyl nitrate concentration and regional transportation in Beijing. *Atmos. Environ*. **2017**, 166, 543-550.

Zhang, G.; Mu, Y. J.; Zhou, L. X.; Zhang, C. L.; Zhang, Y. Y.; Liu, J. F.; Fang, S. X.; Yao, B. Summertime distributions of peroxyacetyl nitrate (PAN) and peroxypropionyl nitrate (PPN) in Beijing: Understanding the sources and major sink of PAN. *Atmos. Environ*. **2015a**, 103, 289-296.

Zhang, Y. L.; Wang, X. M.; Zhang, Z.; Lü, S. J.; Huang, Z. H.; Li, L. F. Sources of C_2–C_4 alkenes, the most important ozone nonmethane hydrocarbon precursors in the Pearl River Delta region. *Sci. Total. Environ*. **2015b**, 502, 236-245.

Zhang, G.; Mu, Y. J.; Liu, J. F.; Zhang, C. L.; Zhang, Y. Y.; Zhang, Y. J.; Zhang, H. X. Seasonal and diurnal variations of atmospheric peroxyacetyl nitrate, peroxypropionyl nitrate, and carbon tetrachloride in Beijing. *J. Environ. Sci*. **2014a**, 26 (1), 65-74.

Zhang, H.; Xu, X.; Lin, W.; Wang, Y. Wintertime peroxyacetyl nitrate (PAN) in the megacity Beijing: Role of photochemical and meteorological processes. *J. Environ. Sci*. **2014b**, 26(1), 83-96.

Zhang, Y. L.; Wang, X. M.; Blake, D. R.; Li, L. F.; Zhang, Z. Wang, S. Y.;Guo, H.; Lee, S. C.; Gao, B.; Chan, L. Y.; Wu, D.; Rowland, F. S. Aromatic hydrocarbons as ozone precursors before and after outbreak of the 2008 financial crisis in the Pearl River Delta region, South China. *J. Geophys. Res：Atmospheres*. **2012**,117, D15306.

Zhang, J. M.; Wang, T.; Ding, A. J.; Zhou, X. H.; Xue, L. K.; Poon, C. N.;Wu, W. S.; Gao, J.; Zuo, H. C.; Chen, J. M.; Zhang, X. C; Fan, S. J. Continuous measurement of peroxyacetyl nitrate (PAN) in suburban and remote areas of western China. *Atmos. Environ*. **2009**, 43(2), 228-237.

Zeng, L. W.; Lyu, X. P.; Guo, H.; Zou, S. C.; Ling, Z. H. Photochemical Formation of C_1–C_5 Alkyl Nitrates in Suburban Hong Kong and over the South China Sea. *Environ. Sci. Technol*. **2018**, 52(10), 5581-5589.